

Privacy in Practice: Private COVID-19 Detection in X-Ray Images

Lucas Lange
lange@informatik.uni-leipzig.de
Leipzig University, Germany

Maja Schneider
mschneider@informatik.uni-leipzig.de
Leipzig University, Germany

Erhard Rahm
rahm@informatik.uni-leipzig.de
Leipzig University, Germany

ABSTRACT

Machine learning (ML) can help fight the COVID-19 pandemic by enabling rapid screening of large volumes of chest X-ray images. To perform such data analysis while maintaining patient privacy, we create ML models that satisfy Differential Privacy (DP). Previous works exploring private COVID-19 ML models are in part based on small or skewed datasets, are lacking in their privacy guarantees, and do not investigate practical privacy. In this work, we therefore suggest several improvements to address these open gaps. We account for inherent class imbalances in the data and evaluate the utility-privacy trade-off more extensively and over stricter privacy budgets than in previous work. Our evaluation is supported by empirically estimating practical privacy leakage through actual attacks. Based on theory, the introduced DP should help limit and mitigate information leakage threats posed by black-box Membership Inference Attacks (MIAs). Our practical privacy analysis is the first to test this hypothesis on the COVID-19 detection task. In addition, we also re-examine the evaluation on the MNIST database. Our results indicate that based on the task-dependent threat from MIAs, DP does not always improve practical privacy, which we show on the COVID-19 task. The results further suggest that with increasing DP guarantees, empirical privacy leakage reaches an early plateau and DP therefore appears to have a limited impact on MIA defense. Our findings identify possibilities for better utility-privacy trade-offs, and we thus believe that empirical attack-specific privacy estimation can play a vital role in tuning for practical privacy.

KEYWORDS

Privacy-preserving machine learning, differential privacy, membership inference attack, practical privacy, COVID-19 detection

1 INTRODUCTION

The COVID-19 pandemic pushed health systems worldwide to their limits, making a rapid detection of infections vital to prevent uncontrollable spreading of the virus. Detecting COVID-19 in patients can be achieved using an RT-PCR test¹. Although they are more reliable in terms of sensitivity than rapid antigen tests, results can take hours to arrive, and even if displaying negative, the virus could have already left the throat and manifested itself in the lungs, rendering it undetectable for either test [4].

In hospitals, chest X-rays can mitigate these drawbacks by enabling a fast and reliable diagnosis [37]. Figure 1 shows chest X-ray scans of healthy (top) and COVID-19 (bottom) patients in direct comparison. Even though patchy consolidations are recognizable in the COVID-19 scans, such X-rays remain challenging to interpret.

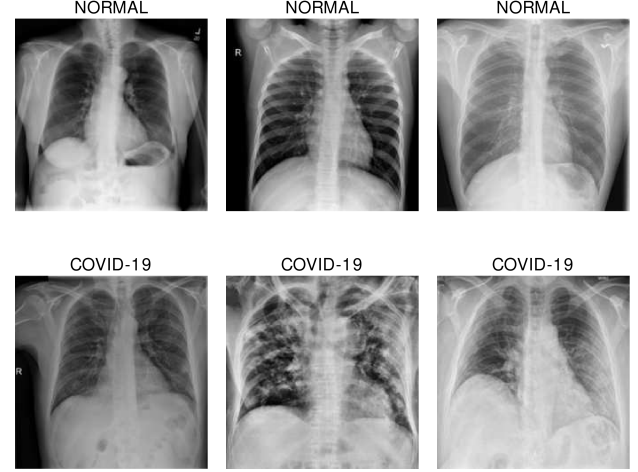


Figure 1: Chest X-ray images of different patients extracted from the COVID-19 Radiography Database [11, 42]. COVID-19 positive scans are characterized by patchy consolidations of the lungs [36].

Specialists, however, are able to identify the severity of a case early on and can take measures without waiting for lab results.

Machine Learning (ML) techniques can effectively assist medical professionals in an initial screening by quickly classifying large numbers of images. However, the amount of data needed for training such classifiers poses problems due to clinical data privacy regulations, which present strict limitations to data sharing between hospitals [6]. All sensitive patient information must be treated confidentially before, during, and after processing. To complicate matters, not only the dataset itself but also the classification models resulting from ML can compromise data integrity. Published models are vulnerable to attacks, including leaking details about their training data [3]. Such leaks allow adversaries to potentially deduce private facts about individuals in the dataset, for instance by exposing the patient’s genetic markers, as shown by Fredrikson et al. [17]. In the case of COVID-19 detection, an attacker could be able to learn if a person was previously infected or not. While the specific risk of X-ray-based attacks might be low, such data should still be handled with caution, especially since even with de-identification results can be linked to other sources of personal information. Further, we cannot rule out an attacker with internal access, e.g. doctors utilizing the classifier inside a hospital.

Privacy-Preserving ML (PPML) are methods for creating trustworthy models, enabling, for example, the development of medical applications while maintaining patient privacy. In this work we

¹Reverse Transcription Polymerase Chain Reaction (RT-PCR) testing is broadly used for COVID-19 diagnosis.

Table 1: Existing solutions from related work next to our best private model. A direct performance comparison is difficult due to the different characteristics. For differentiating the tasks, we assign each method its relevant classes of COVID-19 (C), Normal (N), or Pneumonia (P). For our method, we selected the best performing private model regarding accuracy since related work relies on this metric. Baseline gives the best non-private result, which in our case is achieved by ResNet50 ImageNet. We further include our proposed additions for filling open gaps (F1-score, MIA).

Related Work	Method	Number of samples	Task	Accuracy in %		ϵ	F1?	MIA?
				Baseline	Private			
Müftüoğlu et al. [34]	PATE on EfficientNet-B0	139 COVID-19 234 Normal	binary C N	94.7	71.0	5.98	×	×
Zhang et al. [52]	ResNet on images from DP-GAN trained in federated learning	350 COVID-19 2,000 Normal 1,250 Pneumonia	multi-class C N P	92.9	94.5	?	×	×
Ho et al. [21]	DP-SGD in federated learning on custom CNN with spatial pyramid pooling	3,616 COVID-19 10,192 Normal 1,345 Pneumonia	multi-class C N P	95.3	68.7	39.4	×	×
Lange et al. [ours]	DP-SGD on ResNet18 with tanh activation and pre-training on Pneumonia	3,616 COVID-19 5,424 Normal	binary C N	95.0	77.9	1	✓	✓

apply PPML that satisfies Differential Privacy (DP) in training a COVID-19 detection model, thus limiting attacks on the resulting classifier from incurring information leakage.

Our investigation is divided into three successive steps: (i) First, a non-private baseline is trained to detect COVID-19 vs. Normal (no findings) in chest X-rays. (ii) The second step then focuses on experiments evaluating ML model architectures and parameters in private training, with the primary objective of finding a feasible utility-privacy trade-off. (iii) Finally, model privacy is empirically assessed by attempting the identification of training data through black-box Membership Inference Attacks (MIAs) [45], examining to what extent these models are prone to information leakage.

Our contributions are:

- We fill open gaps from previous work on private COVID-19 detection in X-rays [21, 34, 52]. Table 1 shows their characteristics and drawbacks in comparison to our approach. Existing solutions are in part based on small or skewed datasets, are lacking in their privacy guarantees, and do not investigate practical privacy. We thus adopt methods to incorporate the inherent class imbalances and analyze the utility-privacy trade-off more extensively by evaluating multiple and stricter privacy budgets. We further investigate practical privacy by empirically estimating privacy leakage through black-box MIAs. The gaps and our improvements will be further addressed throughout the following sections.
- We are the first to practically test if DP helps narrow down MIAs on the COVID-19 detection task. We additionally re-examine this hypothesis on the MNIST [29] database to reveal commonalities and differences between the tasks. Our results point towards identifying the benefits from DP in defending against MIAs as task-dependent and plateauing. From these findings, we are able to gain better utility-privacy trade-offs at no practical cost. These results thus strengthen

the belief that empirical privacy analysis can be a vital tool in supporting attack- and task-specific tuning for practical utility-privacy trade-offs.

The following Section 2 provides an overview of essential concepts. We then contextualize our work by examining existing literature in Section 3. In Section 4 we present our selected solutions to address open research gaps. The following part in Section 5 lays out our experimental setup, with the results presented in Section 6 and their discussion in Section 7. In closing, the final Section 8 provides conclusive thoughts and adds an outlook on possible future work.

2 BACKGROUND

This section establishes a basic understanding of the relevant concepts and algorithms used in this work. Within Section 2.1, we first establish a state-of-the-art rigorous notion of privacy and then in Section 2.2 present an algorithm to incorporate such privacy into ML processes. Lastly, Section 2.3 introduces a devastating attack that threatens to leak information from ML models.

2.1 Differential Privacy

An ever-present concept and gold standard in private data analysis is DP, which offers a guarantee that the removal or addition of a single database item does not (substantially) affect the outcome of any analysis [14]. Thus, an attacker is incapable of differentiating from which of two neighboring datasets a given result originates and has to resolve to a random guess—i.e., a coin flip.

DP’s provided guarantee is measured by giving a theoretical upper bound of privacy loss, represented as the privacy budget ϵ . The metric is accompanied by the probability of privacy being broken by accidental information leakage, which is denoted as δ and depends on the dataset size.

Formally, an algorithm A training on a set S is called (ϵ, δ) -differentially-private, if for all datasets D and D' that differ by

exactly one record:

$$\Pr[A(D) \in S] \leq e^\epsilon \Pr[A(D') \in S] + \delta \quad (1)$$

Meaningful privacy guarantees should fulfill $\epsilon \leq 1$ and $\delta \ll 1/n$, where n is the number of training samples in the dataset [9, 35]. The notation $\epsilon = \infty$ is used to indicate that no DP criteria are met.

The design of DP ensuring algorithms is based on one of DP’s fundamental properties: composability. It states that if all the components of a mechanism are differentially-private, then so is their composition [14]. Another essential attribute of DP is its post-processing immunity, implying DP is preserved by all further processing. Therefore, in terms of achieved privacy, it does not matter whether a ML model uses an already DP conform dataset or applies DP while training [16].

2.2 Differentially-Private Stochastic Gradient Descent

The Differentially-Private Stochastic Gradient Descent (DP-SGD) algorithm as proposed by Abadi et al. in [2] takes widely used SGD [43] and applies a gradient perturbation strategy. Gradient perturbation adds enough noise to the intermediate gradients to obfuscate the largest value, since that original sample inhibits the highest risk of exposure [2]. To generally bound the possible influence of individual samples while training, DP-SGD clips gradient values to a predefined maximum Euclidean norm before adding noise. The noisy gradients are then used to update the parameters as usual. The total noise added through the algorithm is composed over all training iterations using an accounting mechanism and determines the resulting privacy budget [2].

2.3 Membership Inference Attacks

In black-box MIAs, an attacker feeds data samples to a target model and thereby tries to figure out each sample’s membership or absence in the model’s training set based solely on the returned confidence values. This technique takes advantage of the differences in predictions made on data used for training versus unseen data, where the former is expected to output higher confidence values due to memorization [9]. As proposed by Shokri et al. in [45], such attacks can utilize multiple shadow models specifically mimicking a target model’s predictions, to train an attack model able to elicit the desired membership information. Salem et al. [44] relaxed the need for shadow models, by finding that simply using the original model’s predictions on given samples can be sufficient to deduce their membership.

The threat of successful MIAs to ML models is immense, because by revealing the membership of an individual’s record in the dataset, they might in turn disclose sensitive information on them. However, the decisive prerequisite for an adversary is some form of existing prior knowledge of the target data, because the MIA can only test samples available to the attacker [45]. Thus, the attacker needs to possess the individual sample to uncover its membership.

3 RELATED WORK

In the following, we first extract gaps left open by related work in Section 3.1. We then follow with an overview of possible mitigation

strategies against MIAs in Section 3.2. The last part in Section 3.3 presents important works regarding practical privacy analysis.

3.1 Private Detection of COVID-19 in X-Rays

In Table 1, existing work on private COVID-19 detection from X-rays [21, 34, 52] is summarized and compared to our approach. There are multiple factors that impede a fair comparison between the listed works, which mainly lie in the substantial differences in datasets, tasks, and privacy guarantees (ϵ). In this section, we will give details on open gaps and then come back to them in Section 4 with elaborations on how these are addressed by this work. We first give a quick overview of the existing methods.

The authors of [34] use the Private Aggregation of Teacher Ensembles (PATE) framework by Papernot et al. [38]. The data is split between multiple teachers that are predicting noisy labels for data that then conforms to DP. A final student model is trained on the resulting private dataset and can then be safely published. As their model architecture, they employ the EfficientNet-B0 [48].

Ho et al. [21, 22] employ an approach that merges DP-SGD and Federated Learning (FL) [32]. They thereby collaboratively train a private model on distributed data sources. Their more recent version [21] adds spatial pyramid pooling [19] to their custom CNN architecture.

Zhang et al. [52] introduce the FedDPGAN, a Differentially-Private Generative Adversarial Network (DP-GAN) that integrates into the FL framework. The scenario describes a DP-GAN that is collaboratively trained using FL and DP-SGD. The resulting GAN-model creates synthetic and private images for training a ResNet [20] student model.

We find the following open gaps:

- *Datasets.* Here, the main problem with [34] is that their result is based on only a small dataset of 139 COVID-19 scans, which could be unrepresentative. The COVID-19 Radiography Database [11, 42] used by Ho et al. [21] and us, provides a better basis in terms of dataset size. However, the imbalances between the classes result in a rather skewed data basis, which is left unaddressed in [21]. With the FedDPGAN, Zhang et al. [52] try to enlarge and balance their small dataset using synthetic images, but the quality of the generated distribution is left unanswered. This is particularly problematic because GANs trained on imbalanced input data tend to produce data with similarly disparate impacts [18]. As a general problem regarding skewness, all of the mentioned works solely assess model performance using accuracy, although this metric is known to undervalue false negatives for minority classes and could favor classifiers that are actually worse in detecting the COVID-19 minority class [8].
- *Privacy budgets.* The used ϵ -values of 5.98 and 39.4 by [34] and [21] respectively, are significantly weaker than the privacy budget of $\epsilon \leq 1$, which is commonly assumed to provide strong privacy [9, 35]. Further, the results by [52] even lack basic comparability, since they do not provide the accumulated privacy loss as a privacy budget in their evaluation and instead only state the used noise scales. Thus, none of the existing models adheres to a strong theoretical privacy

promise and they instead only offer evaluations on weak or unclear privacy guarantees.

- *Practical privacy.* Regarding practical privacy implications, related work does not include actual attack scenarios. It is therefore left unclear to what extent the provided models and ϵ -guarantees retain patient privacy against a real adversary. Such analysis helps in assessing the defense capabilities provided by the achieved privacy budgets and could reveal room for tuning them.

3.2 Repelling Membership Inference Attacks

With a perfect MIA defense, an attacker is unable to distinguish between new samples and samples the model has already seen. Related work suggests multiple different strategies for reducing MIA threats.

As a simple improvement to MIA defense, Shokri et al. [45] show that limiting the model outputs to only return a class label instead of explicit confidence values is a straightforward defense mechanism. But even if effective, they cannot achieve complete mitigation of the attack. In a medical task like COVID-19 detection, where the use case is to help medical professionals in diagnosing a disease, the confidence value is an integral part that indicates how likely a patient is affected. We thus cannot apply the remedy of omitting confidence.

In addition to omitting confidence values Shokri et al. [45] also find that the structure and type of the ML model can contribute to MIA defense. Salem et al. [44] go further and demonstrate that even the training process can help with repelling MIAs. In their experiments, model stacking in the form of ensemble training reduces memorization in the final student model.

In their fundamental work Dwork et al. [15] state that DP should limit and oppose the success of MIAs by design, with Jayaraman and Evans [25] supplying the corresponding reasoning: “[DP], by definition, aims to obfuscate the presence or absence of a record in the data set. On the other hand, [MIAs] aim to identify the presence or absence of a record [...]”. Thus, intuitively these two notions counteract each other.” Rahman et al. [41] test this hypothesis by evaluating MIAs on different privacy levels. They find their model’s resistance to MIAs to gradually increase when lowering the allowed privacy budget. They explain the success of stricter privacy budgets against MIAs with the fact, that models trained at lower ϵ were less prone to overfitting—overfitting being one of the primary culprits behind the success of MIAs [45]. Building a comprehensive study on the topic of overfitting, Yeom et al. [49] prove that overfitting in ML models is sufficient to enable MIAs. At the same time, their formal analysis shows that overfitting is no necessary criterion, and stable models can still hold membership vulnerability.

3.3 Practical Privacy Analysis through Attacks

In recent years, multiple works examined the possibilities of estimating the practical privacy for ML models by performing an empirical study through attacks [9, 24, 25, 31, 35].

Jagielski et al. [24] and Nasr et al. [35] conclude, that the assumed theoretical upper bound privacy loss for DP, given in the privacy budget ϵ , gives a tight worst-case analysis on attack proneness and thereby limits MIA success.

However, in many cases actual attacks extract significantly less information than assumed by the theoretical bound [24, 25, 31, 35]. This discrepancy could possibly enable better utility-privacy trade-offs, but Jayaraman and Evans [25] on the other hand, warn that privacy always comes at a cost and reducing privacy could ultimately promote information leakage. To estimate and investigate the more realistic threat levels, related works empirically measure a model’s practical leakage through attacks, such as MIAs.

Malek et al. [31] propose that a lower bound on the amount of revealed information by a model can be determined by “[considering] the most powerful attacker pursuing the least challenging goal” and that in the case of standard DP, such would be an attacker powerful enough to perform the goal of membership inference. Thus, by attacking our models with MIAs, we can empirically estimate a more realistic lower bound of practical privacy leakage which might differ substantially from the upper privacy leakage bound derived from DP theory.

4 METHODS

As described in Section 3.1 and shown in Table 1, related work on COVID-19 detection lacks comparability and leaves open gaps [21, 34, 52]. We therefore do not solely focus on enhancing the performance of existing model architectures but rather suggest improvements by filling research gaps.

We propose the following improvements:

- *Datasets.* Since the dataset used by us and Ho et al. [21] provides a good amount of COVID-19 samples, we instead aim for better handling of the problems arising from the skewed nature of the dataset distribution. In a first effort, we employ random undersampling [13, 33] and class weights [53] to elevate the underrepresented COVID-19 class, both in database construction and in training, respectively. We ensure reproducibility throughout the dataset construction process by utilizing fixed a random seed in our implementation. As a further measure, since accuracy is no representative measurement in cases of skewed data, we improve the evaluation by introducing the more balanced F1-score metric [8].
- *Privacy budgets.* We better investigate the utility-privacy trade-off by evaluating multiple and stricter privacy budgets of $\epsilon = \infty$, $\epsilon = 10$, $\epsilon = 1$, and $\epsilon = 0.1$. To achieve our private models, we extend the pool of evaluated methods by utilizing centralized DP-SGD and proposing multiple untested architectural experiments relevant to private training, as presented in Section 5.4.
- *Practical privacy.* As seen in the works discussed in Section 3.3, we investigate the practical implications of DP regarding the defense against black-box MIAs by undertaking an empirical analysis through actual attacks and thus give a more realistic lower bound to the resulting privacy leakage [24, 31]. We thereby provide the first attack results in the field of private COVID-19 detection and evaluate possible room for tuning the utility-privacy trade-off. An additional evaluation regarding the privacy leakage of our models on the MNIST database [29], enables us to formulate takeaways regarding similarities and disproportions regarding the attack-specific privacy on both datasets. Evaluating another

Table 2: Summary of the parameters and settings used in the experiments. Each combination from left to right constitutes a possible setup for a model variant.

Dataset	Architecture	Activation	Pre-training	ϵ
COVID-19	ResNet18	ReLU	None/Standard	∞
MNIST	ResNet50	tanh	ImageNet	10
			Pneumonia	1
				0.1

dataset is a first step towards generalization and MNIST is particularly interesting because related works [35, 41] previously investigated the connection between DP and MIA on this task, see Sections 3.2 and 3.3 for details on their findings.

5 EXPERIMENTAL SETUP

Table 2 summarizes the different configurations used in our experiments. In this section, we provide more background and details on these setups.

5.1 Environment

Our language of choice for the implementation is Python, with ML workflows created using the Keras [10] deep learning API running on top of Google’s Tensorflow [1] framework. Further, we employ the modules for DP-SGD training and MIAs from the Tensorflow Privacy library². To enable consistency and allow reproducible results, random seeds are set to a fixed value, which is 42 in our case. Hardware-wise our machines are equipped with 32GB of RAM and an NVIDIA Tesla V100 GPU.

5.2 Datasets

For a comprehensible dataset creation, we provide details on the different public datasets used in our data gathering phase.

- The *COVID-19 Radiography Database* [11, 42] found on Kaggle³ is the most comprehensive collection of COVID-19 chest X-ray images, stemming from different databases around the web. Next to COVID-19, it contains images of Normal and Pneumonia cases. In total, this image collection offers chest X-rays of 3,616 COVID-19 positive, 10,192 Normal, and 1,345 Pneumonia cases. For the task of differentiating COVID-19 vs. Normal, we only keep these two classes. To directly mitigate some of the clear imbalances we employ undersampling and the final dataset construction takes all COVID-19 scans but only 1.5× the amount for Normal (5,424), resulting in a total of 9,040 images.
- The *Chest X-Ray Images (Pneumonia)* [26] is another Kaggle dataset⁴ but containing only Normal and Pneumonia images. It offers 5,856 X-ray images divided into two categories as 1,583 Normal and 4,273 Pneumonia samples. Here, undersampling results in the final dataset taking all Normal scans but just 1.5× the amount for Pneumonia (2,374).

The Chest X-Ray Images (Pneumonia) set is also part of the COVID-19 Radiography Database, constituting 13% (1,341) of its Normal class images. To fix this issue and enable its use as a public dataset for our private transfer learning approach without compromising privacy, we exclude the duplicates when sampling images for the COVID-19 task.

- The *ImageNet* [12] is a vast collection counting 14 million images and covering 20,000 categories from general (mammal) to specific (husky). Non-private models are found to benefit from using this massive dataset for pre-training, introducing many differentiating concepts to a neural network before training on the target data [23].
- With their *MNIST Database* [29], LeCun et al. offer a large image collection of handwritten digits. The database provides 60,000 images for training and 10,000 for testing. Even though this database does not contain COVID-19 related images, MNIST is a commonly used benchmark in image classification and PPML, making it a perfect candidate for comparing results, see e.g. [2, 5, 9, 35, 38–41, 45, 49, 51].

The experiments are mainly focusing on the task-relevant COVID-19 Radiography Database as the evaluation basis. Additionally, models are then evaluated on the MNIST database and task. Any pre-training uses the respective public ImageNet and Pneumonia datasets.

5.3 Pre-processing

To build our final splits for model training, we employ necessary sampling and pre-processing steps. Both X-ray datasets, for COVID-19 and pneumonia, use a train-validation-test split of 80-5-15, i.e., 80% of images form the training set, 5% the validation set, and 15% the test set. All datasets are handled with three color channels. We therefore convert the MNIST grey-scale images to the RGB space, as this is vital to allow the models pre-trained on color images to still work with the input data. Furthermore, each data point undergoes a normalization step by scaling each image by a factor of $x=1/255$.

To combat overfitting, training sets are shuffled and training images from the X-ray datasets are subjected to data augmentation [46]. The applied random mechanisms and parameters are horizontal flip, rotation $\pm 10\%$, translation $\pm 10\%$, zoom $\pm 15\%$, and brightness $\pm 10\%$. Random brightness alteration is particularly interesting for the use with X-ray scans.

An earlier problem stemming from the X-ray datasets’ construction is their imbalance regarding Sickness (COVID-19, Pneumonia) and Normal class frequencies. In both cases, the sets contain 1.5× more Normal images after already undersampling the class. Consequently, models could favor the Normal cases and treat Sickness as an unimportant minority to gain better results. To reduce the impact of this issue, we apply class weights to help artificially restore the balance while training [53]. When calculating the values for each class, class frequencies are taken and translated into factors that equalize each class’s impact on model updates. This process yields class weights of 0.83 for the Normal and 1.25 for the Sickness classes.

²GitHub: <https://github.com/tensorflow/privacy>

³Kaggle: <https://www.kaggle.com/tawsifurrahman/covid19-radiography-database>

⁴Kaggle: <https://www.kaggle.com/paultimothymooney/chest-xray-pneumonia>

5.4 Architectural Experiments

In the following, we describe our different architectural choices for the experiments.

5.4.1 Model size in DP-SGD. Non-private and private classification perform differently depending on the underlying model architecture [7, 40]. Performance is greatly dependent on model size, i.e., the number of layers or parameters in a model, with non-private training typically benefiting from using bigger models. In contrast, using DP-SGD, the same models suffer from accuracy loss when increasing in size. Taking these findings into account, the experiments use two differently-sized architectures.

5.4.2 ResNets. The model family of Residual Networks [20], or ResNets, provides well-scaling deep CNN architectures thanks to its residual connections. We utilize two different versions as our basic model architectures for the experiments. For one, the ResNet50 version boasting 50 layers, which is a stretched compromise between size and computing needs, as well as the ResNet18, which is mostly identical except for the lower layer count. When introducing architectural experiments, we change each basic model accordingly, creating different variants.

5.4.3 Pre-training. An important consideration in private training is the use of public pre-training datasets. This is due to the advantage that public datasets do not require the same noisy training mechanisms as private datasets. On the basis of the resulting pre-tuned weights, the pre-trained model is then fine-tuned to the private target data for the actual task.

A commonly applied strategy in non-private classification is a general pre-training using the extensive ImageNet collection, which usually leads to better performance [23]. As another method, Abadi et al. [2] state that DP-SGD models can further profit from pre-training in a domain closely related to the target task. So, while the ImageNet resembles more of a general choice for image-based tasks, a pre-training for pneumonia detection is more relevant to our COVID-19 task due to the similarity in symptoms [28, 47].

The pre-training on the Pneumonia dataset is performed using the same settings as on the COVID-19 set, while the ImageNet variants are provided by a Python library that extends the existing range of Keras models⁵.

5.4.4 tanh activation. A disruptive discovery in DP-SGD research was made by Papernot et al. [40]. In their work, they determined that replacing the de facto standard ReLU activation function with the tanh function in model layers improves performance in DP-SGD. To achieve this boost, they utilize the fact that the tanh activation generally results in smaller gradients than the ReLU function, which in turn reduces the information loss from gradient clipping.

5.5 Parameters of Model Training

In this section, we elaborate on the used settings and hyperparameters for the experiments.

5.5.1 General settings. Models train for 20 epochs, employ batch sizes of 32, and use the Adam optimizer [27], a decision mainly due

to Adam’s adaptive properties, enabling it to perform similarly to a task-adjusted SGD in non-private and private training [40].

The starting learning rate for each scenario is $\alpha = 1e-3$, which then decays on plateaus, i.e., if the loss on the validation set does not improve for two consecutive epochs, the learning rate is reduced by one magnitude up to a minimum of $\alpha = 1e-6$. The decay enables finer steps in the parameter updates during further stages of the learning process [50].

For the binary classification task on X-ray images, the models are equipped with a 1-unit output layer with sigmoid activation. Running experiments on MNIST requires models to switch to the multi-class task of differentiating ten digits and thus to a 10-unit output with softmax activation.

5.5.2 DP settings. In theory, we aim at privacy budgets of $\epsilon \leq 1$, since such values present strong privacy guarantees [9, 35]. We therefore focus on $\epsilon = 1$ but also evaluate budgets neighboring this setting by an order of magnitude, to allow further insights into the performance and estimated privacy on different DP levels. Consequently, the evaluation considers models trained for $\epsilon = 0.1$, $\epsilon = 1$, and $\epsilon = 10$, which then stand in contrast to the non-private results at $\epsilon = \infty$. Our theoretical analysis employs the moments account [2] to track moments of privacy loss. In correspondence to the COVID-19 dataset size, the analysis needs to satisfy $\delta \leq 1/n$ for $n = 9,040$, resulting in $\delta = 1e-4$. On the MNIST database in turn, the larger amount of data ($n = 60,000$) asks for $\delta = 1e-5$.

5.5.3 DP-SGD settings. All model variants are first trained non-privately to form a baseline. Afterwards, we apply DP-SGD training to each model, training a private candidate for each ϵ -guarantee. The DP-SGD algorithm simply stacks on top of the existing non-private training by changing the optimizer and handing in the necessary privacy parameters. Although referenced as DP-SGD, our employed optimizer is the accordingly modified DP-Adam version and uses the same learning as non-private training. The needed noise scale for each guarantee is drawn from a Gaussian noise mechanism and varies according to the desired privacy budget. The noise also depends on the utilized batch size, where DP-SGD training for COVID-19 detection uses ResNet50 and ResNet18 variants with batch sizes of 8 and 16, respectively, instead of 32. Finally, we employ a clipping norm of 1.0 to the gradients.

5.5.4 MIA settings. We use the MIA based on logistic regression from the Tensorflow Privacy library, which is an implementation of the single shadow model black-box attack proposed by Salem et al. [44], which directly relies on target model outputs. Given a target model, MIAs utilize two types of data for training: (i) original training data to be inferred and (ii) unseen but similar data to differentiate non-training data. In our case, we want to fully empower the attacker for estimating the practical worst-case in an optimal black-box setting [31]. We satisfy this condition by giving access to the full original training and test sets along with their corresponding correct labels, thus, handing the attacker the largest input regarding (i) and the most similar input regarding (ii).

⁵GitHub: https://github.com/qubvel/classification_models

5.6 Measuring Privacy Leakage

Like Jayaraman et al. [25], our used metric for privacy leakage through MIAs is the achieved membership advantage for the attacker as introduced by Yeom et al. [49].

As a formal foundation, they describe an adversarial game based on an attacker’s capabilities in differentiating the membership of a sample that is chosen uniformly at random to originate from the training set or not. The resulting difference between the adversary’s true and false positive rates for this game is then given as the membership advantage. For example, with an advantage of 0.4, an attacker would be right in 40% more cases than wrong, which converts to 70% correctly identified cases and 30% failures. The 40% thus represents the attacker’s expected information gain compared to random guessing. Random guesses would translate to a minimum advantage of 0.0, since the attacker would be right as often as wrong. The maximum of 1.0 would be a perfect attacker that never fails to identify the correct membership.

In [49], Yeom et al. prove that if a learning algorithm satisfies ϵ -DP, then the adversary’s membership advantage given as Adv^M is bounded by $\text{Adv}^M \leq e^\epsilon - 1$. When transferring the theorem to (ϵ, δ) -DP given by Equation (1), we derive the upper bound as:

$$\text{Adv}^M \leq e^\epsilon - 1 + \delta \quad (2)$$

We refer the reader to Appendix A for a proof of this equation.

Since individual MIA results are subject to variability, they need to be experimentally stabilized. Inspired by Malek et al. [31], we achieve this by running 100 entire MIA experiments and calculating the corresponding 95% Confidence Interval (CI) for the results.

6 RESULTS

In this section, we present the outcomes of our experiments on the COVID-19 and MNIST tasks in Sections 6.1 and 6.2, respectively, and highlight important parts for evaluation. Because of the reasoning given in Section 4, we value F1-score higher than accuracy when comparing model performance.

6.1 Results on the COVID-19 Database

Focusing on the COVID-19 task, Table 3 summarizes the experimental results regarding performance (accuracy, F1-score) and practical privacy (empirical privacy leakage) over the different privacy levels.

When inspecting the $\epsilon = \infty$ columns, the non-private baseline performance is dominated by the ImageNet variants, reaching 93.5% F1 for ResNet18 and ResNet50 alike. Although the ImageNet pre-training also reigns supreme in the tanh versions, they cannot reach the same performance with a maximum of 91.5% F1. The non-private tanh models generally show to underperform compared to their ReLU counterparts, making tanh less suited than ReLU for non-private training. Pneumonia pre-training does not present the same clear improvements as ImageNet and rather sees mixed results, with only the ResNet18 Pneumonia improving by 1.4% compared to the Standard model.

For the first private results examined at $\epsilon = 10$, we already find a steep utility-privacy trade-off of 18.7% compared to the non-private results, with the best F1-score falling from 93.5% to 74.8%. While the ResNet18 ImageNet keeps the best accuracy by a small margin (77.5% vs. 75.8%), it is clearly outperformed by the tanh-Pneumonia

variant in terms of F1-score (62.1% vs. 74.8%). Other than in the non-private setting, the private tanh variants now surpass their ReLU siblings in all cases. The ResNet50 models relying on the ReLU function struggle so much, that they are not able to learn a working classification model (0.0% F1). For both ResNet18 and ResNet50, the tanh-ImageNet falls behind the other tanh candidates, while the Pneumonia pre-training now delivers the best results.

Our results at $\epsilon = 1$ present an even more substantial paradigm shift. First, the ResNet18 ImageNet joins the ResNet50 ReLU variants and is not able to produce a working model at this level. Further, the only two working ReLU models of ResNet18 Standard and Pneumonia see their F1 score plummet to 13.6% and 17.4%, respectively, probably making them unfeasible. Thus, at this lower privacy setting of $\epsilon = 1$, the tanh activation is essential to achieve feasible models for in all variants. We see the ResNet18 tanh-Pneumonia as the best performing model with 74.1% F1 and 77.9% accuracy. From $\epsilon = 10$ to $\epsilon = 1$, we trade off just 0.7% F1, while accuracy even increased by 0.4%.

At the last setting of $\epsilon = 0.1$, we find the return of the ReLU ImageNet variants, in both ResNet18 and ResNet50. Additionally, the tanh-ImageNet models also see an increase in performance, with the ResNet50 version even reaching the second highest F1. Their surprising return might indicate that the relationship between noise and utility might be manifold and not as strictly linear. The best performance, however, is now given by the ResNet50 tanh-Pneumonia at 70.7% F1 and 74.4% accuracy. The resulting trade-off of 3.4% F1 compared to $\epsilon = 1$ is more substantial than the 0.7% between $\epsilon = 10$ to $\epsilon = 1$.

A factor previously neglected in this analysis is the practical privacy represented by the empirical estimation of privacy leakage from MIAs. Here, an interesting finding is that we already see nearly the same values in the non-private settings as in all three private settings. The initial observation holds true when looking at the mean estimate across the privacy levels, which would be 0.12–0.13 for $\epsilon = \infty$, 0.12–0.14 for $\epsilon = 10$, 0.12–0.13 for $\epsilon = 1$, and 0.12–0.13 for $\epsilon = 0.1$ —almost all the same.

6.2 Results on the MNIST Database

We omit the Pneumonia variants from this evaluation, since Pneumonia does not constitute a related task to MNIST. The results for the remaining models are shown in Table 4, where they are again compared by accuracy, F1-score, and estimated privacy leakage.

The non-private performance trends show that MNIST is an easier task than COVID-19 detection because only one model falls short of reaching the 99% F1 mark. Furthermore, the tanh models are on par with the ReLU models even in the non-private setting. Familiarly to the COVID-19 task, the ResNet18 ImageNet performs best at 99.4% F1.

In private training, the ResNet50 again fails to deliver feasible ReLU models at $\epsilon = 10$. The other models, however, only see a smaller reduction in their performance than before for COVID-19. The ResNet18 tanh-ImageNet achieves the best result at 98.1% F1, a 1.3% reduction from $\epsilon = \infty$. ResNet50 tanh-ImageNet closely follows at 97.6% F1, making the tanh-ImageNet overall the best private variants at $\epsilon = 10$.

Table 3: Experimental results on the COVID-19 dataset. Each ResNet18 and ResNet50 variant is evaluated across multiple DP budgets (ϵ)—where $\epsilon = \infty$ translates to non-private training. Private models result from DP-SGD training. The Standard, ImageNet and Pneumonia models rely on the ReLU activation function, which is then changed to tanh in the respective counterparts. All variants are matched by their classification accuracy and F1-score in %, as well as, their empirical privacy leakage derived from MIAs, which is measured by the method explained in Section 5.6 and given as a 95% CI over 100 attacks. If training did not result in a feasible model, leading to an F1-score of 0.0, no accuracy is given and no attacks are performed (NA). The experiments are summarized in Table 2 and further explained in Section 5.

Variant	$\epsilon = \infty$			$\epsilon = 10$			$\epsilon = 1$			$\epsilon = 0.1$		
	%-Acc.	%-F1	Leakage	%-Acc.	%-F1	Leakage	%-Acc.	%-F1	Leakage	%-Acc.	%-F1	Leakage
ResNet18												
Standard	91.5	89.3	0.13–0.14	74.2	64.4	0.13–0.14	61.5	13.6	0.12–0.13	NA	0.0	NA
ImageNet	95.0	93.5	0.11–0.12	77.5	62.1	0.14–0.16	NA	0.0	NA	51.5	61.0	0.12–0.13
Pneumonia	93.4	91.7	0.13–0.14	69.8	52.3	0.12–0.13	61.4	17.4	0.12–0.13	NA	0.0	NA
tanh-Standard	82.0	81.2	0.12–0.13	73.5	72.6	0.12–0.14	73.5	67.8	0.13–0.14	69.3	65.0	0.13–0.14
tanh-ImageNet	91.5	89.9	0.12–0.13	63.4	68.4	0.12–0.13	43.6	58.5	0.12–0.13	49.9	60.6	0.13–0.14
tanh-Pneumonia	79.7	78.5	0.12–0.13	75.8	74.8	0.13–0.14	77.9	74.1	0.13–0.14	70.6	60.5	0.12–0.13
ResNet50												
Standard	92.5	90.5	0.12–0.13	NA	0.0	NA	NA	0.0	NA	NA	0.0	NA
ImageNet	94.8	93.5	0.11–0.12	NA	0.0	NA	NA	0.0	NA	40.4	55.5	0.12–0.13
Pneumonia	91.4	89.6	0.12–0.13	NA	0.0	NA	NA	0.0	NA	NA	0.0	NA
tanh-Standard	81.6	80.7	0.13–0.14	72.8	63.1	0.12–0.13	71.2	64.6	0.13–0.14	61.4	61.4	0.12–0.13
tanh-ImageNet	87.7	84.8	0.13–0.14	47.6	60.2	0.12–0.13	46.9	59.5	0.12–0.13	72.6	65.1	0.12–0.13
tanh-Pneumonia	80.0	77.8	0.13–0.14	67.1	69.9	0.12–0.13	71.8	72.2	0.12–0.13	74.4	70.7	0.12–0.13

Table 4: Experimental results on the MNIST database. See Table 3 caption for details on the contents. Because of the multi-class task F1-score is given as the macro average over the 10 output classes. We omit the models with pneumonia pre-training from the MNIST evaluation, since the two tasks are not closely related.

Variant	$\epsilon = \infty$			$\epsilon = 10$			$\epsilon = 1$			$\epsilon = 0.1$		
	%-Acc.	%-F1	Leakage	%-Acc.	%-F1	Leakage	%-Acc.	%-F1	Leakage	%-Acc.	%-F1	Leakage
ResNet18												
Standard	99.1	99.1	0.33–0.37	96.0	96.0	0.13–0.14	92.3	92.2	0.12–0.13	23.0	18.0	0.13–0.13
ImageNet	99.4	99.4	0.37–0.42	95.4	95.3	0.13–0.14	84.1	83.6	0.13–0.14	16.3	14.5	0.11–0.12
tanh-Standard	99.3	99.3	0.37–0.41	95.9	95.8	0.13–0.14	92.2	92.0	0.12–0.13	72.7	71.3	0.13–0.14
tanh-ImageNet	99.0	99.0	0.27–0.32	98.1	98.1	0.16–0.18	97.1	97.0	0.14–0.16	93.8	93.5	0.13–0.13
ResNet50												
Standard	99.3	99.3	0.34–0.38	16.4	14.3	0.11–0.12	13.6	12.9	0.11–0.12	11.2	9.4	0.11–0.12
ImageNet	99.2	99.2	0.43–0.48	10.6	9.5	0.12–0.12	10.0	9.1	0.11–0.12	9.5	8.0	0.11–0.12
tanh-Standard	99.2	99.2	0.32–0.36	93.6	93.4	0.12–0.13	87.4	87.2	0.12–0.13	30.6	27.4	0.12–0.13
tanh-ImageNet	98.4	98.4	0.26–0.30	97.6	97.6	0.15–0.17	96.6	96.6	0.13–0.15	92.8	92.3	0.12–0.13

Their superiority carries over to $\epsilon = 1$, where we mostly see the same ranking of models, with the ResNet18 tanh-ImageNet reigning and delivering 97.0% F1. This results in a small F1 trade-off of 1.1% from $\epsilon = 10$ to $\epsilon = 1$.

The minimal trade-off cannot be kept for $\epsilon = 0.1$, where the ResNet18 tanh-ImageNet stays on top but loses 3.3% F1 and lands at 93.5%. The total F1 trade-off from $\epsilon = \infty$ to $\epsilon = 0.1$ is still low at 5.9% and presents a substantially better trade-off than on the COVID-19 task. F1 for ResNet18 Standard and ImageNet decreases steeply at

$\epsilon = 0.1$, delivering rather unusable models. Even the tanh-Standard falls to a low of 27.4% F1.

Shifting the view to the results for our practical privacy analysis, non-private models on MNIST show a significantly higher proneness to MIAs than on COVID-19 detection. The mean leakage in the non-private setting climbs to 0.34–0.38, an almost 3× higher upper bound on the mean than for COVID-19. In stark contrast to the COVID-19 results, we measure an astonishing reduction in mean leakage from introducing DP, leading to 0.13–0.14 at $\epsilon = 10$,

0.12–0.14 at $\epsilon = 1$, and 0.12–0.13 at $\epsilon = 0.1$ —an improvement of over 60%. We thus only find a negligible difference in estimated leakage between the private models on COVID-19 and MNIST. Furthermore, the mean values on MNIST are almost the same in all private settings, just like on the COVID-19 task.

7 DISCUSSION

We now revisit the open research gaps in related work discussed in Section 3 and review the outcomes of our proposed solutions from Section 4. We again refer to Tables 3 and 4 for our evaluation results and to Table 1 for a short and organized showcase of the compared methods from related work [21, 34, 52].

We evaluate our proposed improvements:

- *Datasets.* For training our models, we achieve a more balanced data basis than before by utilizing undersampling and class weights. To better evaluate on the still skewed data basis, we added the F1-score to our performance metrics. The advantage over accuracy is visible from the COVID-19 results, where e.g. at $\epsilon = 10$ accuracy slightly favors the ResNet18 ImageNet, while the F1-score clearly suggests the ResNet18 tanh-Pneumonia that is thus revealed to perform significantly better on the minority class (COVID-19). That F1 better represents the results based on the underlying class distribution is further demonstrated by comparison to the results on MNIST. Because of the more balanced MNIST dataset, accuracy and F1-score are closely related in these experiments.
- *Privacy budgets.* In contrast to related work, we were able to achieve working COVID-19 detection models, while adhering to strong privacy budgets of $\epsilon \leq 1$ [9, 35]. By evaluating multiple architectures over the course of multiple privacy levels, we were able to deduce favorable architectural decisions for keeping good utility-privacy trade-offs in DP-SGD. The resulting findings for training private models are summarized in Section 7.1.
- *Practical privacy.* Taking into account an empirical study on practical privacy through MIAs, we gained insights into the relationship between DP and privacy leakage. The results allowed us to improve the utility-privacy trade-off while keeping the same practical privacy. In Section 7.2 we derive the implications stemming from our empirical analysis.

7.1 Building Better DP-SGD Models

In the following, we denote our findings towards better architectural decisions for DP-SGD training.

With our experiments, we transferred the results from [40] to deeper and pre-trained networks and were able to confirm the clear advantage of tanh over ReLU in DP-SGD training. All our best private models rely on this simple change, while the non-private models still prefer the ReLU activation function.

Another commonality between the best performers is that they were all subjected to pre-training. While the best non-private models are pre-trained on ImageNet, this trend is only found for private models on MNIST, where the tanh-ImageNet performs best. The same tanh-ImageNet models underperform on the COVID-19 task, which might be related to the fundamentally different contents

of the two tasks. On the COVID-19 task, we instead introduced task-specific pre-training as proposed in [2]. The pre-training on pneumonia images lead to the tanh-Pneumonia models that showed to be superior to the other variants in the private settings.

We could, however, not fully confirm that larger models perform worse in DP-SGD [7, 40]. The ResNet18 wins in all cases except for one, which is at $\epsilon = 0.1$ on the COVID-19 task, where the ResNet50 takes the lead. Model size also seems to play a role, when examining the earlier failure of the private ReLU models in the bigger ResNet50.

In summary, our results further support the existing belief that model architectures should be specifically adjusted for private DP-SGD training, where established standards from non-private training do not necessarily provide the same advantages [2, 7, 40]. Examples are the change from ReLU to tanh activation and the superiority of the Pneumonia pre-training to the ImageNet pre-training in the private COVID-19 models.

7.2 Connecting the Dots Regarding Practical DP

For this section, we refer to Figures 2a and 2b that visualize the results for our estimated privacy leakage from MIAs at the different ϵ -budgets.

For COVID-19 in Figure 2a, the leakage almost describes a flat line over all privacy settings. Even the non-private models exhibit the same leakage as the private models and thus, including DP-guarantees does not imply improvements to the practical MIA proneness on this task. The results on the MNIST task in Figure 2b, on the other hand, show a stern reduction in MIA success related to the introduced DP. The non-private MNIST models show to leak significantly more information than the COVID-19 models. However, on MNIST the inclusion of DP clearly reduces the privacy leakage, that then reaches the same levels as on the COVID-19 task. The initial difference in MIA risk between COVID-19 and MNIST suggests, that privacy estimation can be an important tool for assessing task- and data-dependent threats from attacks. Liu et al. [30] also confirmed that MIA success is related to the underlying dataset and task. Thus, such estimates can in turn support tuning trade-offs according to task-specific privacy needs.

Unlike the non-private models, the private models for both tasks almost all show equivalent results once trained for DP. Only the tanh-ImageNet variants on the MNIST task need stronger DP-levels to reach the same low leakage. The general trend of the other models shows them already reaching an early plateau at $\epsilon = 10$. After that, stricter privacy budgets do not further improve practical privacy. The plateau in privacy leakage enables us to use worse DP-guarantees, while still providing the same practical privacy.

To put our results into context we use the proven (ϵ, δ) -DP bounds for our leakage metric given by Equation (2) in Section 5.6. With $\delta = 1e-4$ for COVID-19 and $\delta = 1e-5$ for MNIST, its influence on the leakage bound is negligible in our case. The retrieved limits on the leakage are 22,025 for $\epsilon = 10$, 1.72 for $\epsilon = 1$, and 0.105 for $\epsilon = 0.1$. For $\epsilon = \infty$ we have to assume ∞ accordingly. Since the maximum of leakage is 1.0, out of our budgets, only $\epsilon = 0.1$ would be able to bound the information loss from our attack in the theoretical worst-case.

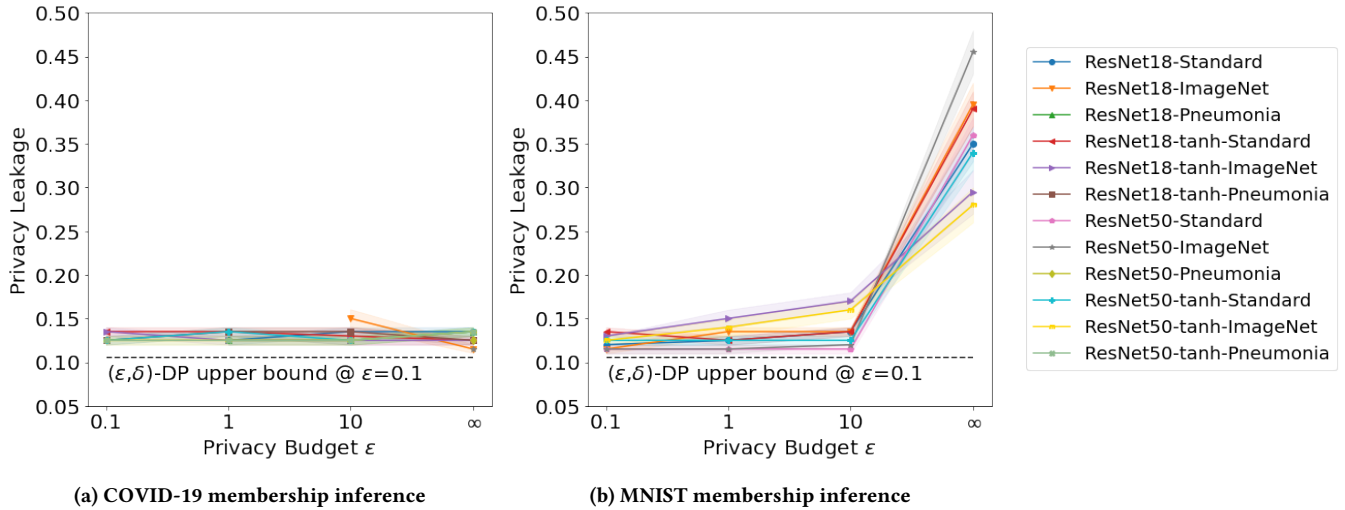


Figure 2: Experimental results regarding practical privacy against MIAs. Empirical privacy leakage is shown across the different privacy budgets. Each model is represented by a colored line with different markings for the recorded results as shown in the legend. Privacy leakage is measured based on the methods explained in Section 3.3. The dotted line shows the corresponding theoretical limit of leakage from (ϵ, δ) -DP at $\epsilon = 0.1$. We plot this line across all privacy budgets to put the leakage into perspective.

In Figures 2a and 2b, we include a dotted line showing the leakage bound for $\epsilon = 0.1$ at the respective δ for each dataset. Even the models at higher ϵ -guarantees are close to this strong privacy bound, which shows the large discrepancy between the theoretically assumed worst-case and practice. Simultaneously, no model trained for $\epsilon = 0.1$ is truly able to conform to the calculated limit, although some models almost match it on their lower CI-bounds. Such inconsistencies can also be found in related work [25, 49]. As an explanation Yeom et al. [49] unveil, that the training set error distributions are not exactly Gaussian, sometimes leading to better attack performance than predicted by theory. Even though COVID-19 and MNIST have rather opposing priors, where the former’s classes are skewed and the later’s roughly balanced, we see the same inconsistencies in both evaluations. Thus, the theoretical bound does not seem reliable for deriving a limit on the real world threat in our case.

The findings suggest room for utilizing weaker DP-guarantees when defending against MIAs on both tasks. Comparing to the respective DP-guarantees, we saw that practical privacy is already strong in our less private models. Furthermore, practical privacy on COVID-19 plateaus for all privacy levels, showing not influence from DP when defending our attack on this dataset. On MNIST, in turn, DP is needed to mitigate the initial proneness of the models, but can be loosened due to the same plateau found for COVID-19. We are thus able to improve the utility-privacy trade-off on both datasets at no practical privacy cost.

Concluding this part of the discussion, we want to emphasize that there can still be a need for strong theoretical privacy guarantees [35]. As seen in Section 3.2, ϵ -guarantees from DP limit the maximum amount of possible information leakage. In actual attacks, however, the theoretical ceiling might differ from the practical threat as shown in this and other works presented in Section 3.3.

From this, we should not conclude that DP is unnecessary, since future adversaries could find better attacks that make an earlier empirical evaluation invalid. To cover for such cases it is therefore advised to keep a reasonably strong privacy guarantee when tuning for better trade-offs. Thus, we would rather choose a COVID-19 model at $\epsilon = 10$ than at $\epsilon = \infty$, even though both exhibit the same practical privacy. The model at $\epsilon = 10$ performs better than the one at $\epsilon = 1$ and, in contrast to $\epsilon = \infty$, still provides a provable DP guarantee.

8 CONCLUSION

Within this piece of work, we closed several open research gaps in the field of private COVID-19 detection from X-ray images. In comparison to related work on the topic, we improved data handling regarding imbalances, delivered a more robust privacy evaluation, and were the first to investigate the implications concerning practical privacy [21, 34, 52].

We introduced a selection of yet untested architectural model choices to the COVID-19 task. Through our evaluation, we were able to compare the setups in a common environment. Since well-known practices from non-private training are not always transferable to DP-SGD training, it is important to gather a wide range of results for finding the best solutions. We are therefore making a noticeable contribution by exploring a range of different architectures on the COVID-19 and MNIST tasks.

Our practical privacy analysis revealed that assessing attack-specific threats from black-box MIAs in a practical scenario helps finding appropriate privacy attributes and can thus improve the utility-privacy trade-off at no practical cost. On the COVID-19 task, we found no obvious connection between the provided theoretical DP-guarantee and practical defense against MIAs. Instead, our

tested models virtually showed the same strong repelling properties across all privacy levels—even for non-private models. Further experiments on the MNIST database showed that practical privacy analysis is important for identifying the initial MIA threat, since non-private models were prone to leak information on this task. However, the introduction of DP significantly increased MIA defense in the MNIST case, which also reached an early plateau that was consistent with the low leakage levels on the COVID-19 task. By confirming the plateau for both data sets, we were able to reduce the required DP guarantees for both tasks without sacrificing practical privacy.

We still advocate the use of DP and would not recommend to risk publishing non-private COVID-19 detection models. Instead, if justified by a practical privacy analysis, the ϵ -guarantee can be tuned to a favorable trade-off that through DP still limits the worst-case information leakage.

In a brief outlook into possible future work, it would be beneficial to extend our evaluation by applying practical privacy analysis to more datasets, especially with different underlying tasks. Another venture could be to derive best practices and ultimately a taxonomy regarding architectural decisions in DP-SGD training.

AVAILABILITY

Reference code for implementation of the experiments is available from our repository at <https://github.com/luckyos-code/mia-covid>.

ETHICAL PRINCIPLES

All patient data originated from public sources provided for research purposes and was solely used within the limited scope of this work.

ACKNOWLEDGMENTS

We thank Peter Christen from The Australian National University and our colleagues at Leipzig University and ScADS.AI for their insightful comments on drafts of this work. The authors acknowledge the financial support by the Federal Ministry of Education and Research of Germany and by the Sächsische Staatsministerium für Wissenschaft, Kultur und Tourismus for ScADS.AI. Computations for this work were done (in part) using resources of the Leipzig University Computing Centre.

REFERENCES

- [1] Martin Abadi, Ashish Agarwal, Paul Barham, Eugene Brevdo, Zhifeng Chen, Craig Citro, Greg S. Corrado, Andy Davis, Jeffrey Dean, Matthieu Devin, Sanjay Ghemawat, Ian Goodfellow, Andrew Harp, Geoffrey Irving, Michael Isard, Yangqing Jia, Rafal Jozefowicz, Lukasz Kaiser, Manjunath Kudlur, Josh Levenberg, Dandelion Mané, Rajat Monga, Sherry Moore, Derek Murray, Chris Olah, Mike Schuster, Jonathon Shlens, Benoit Steiner, Ilya Sutskever, Kunal Talwar, Paul Tucker, Vincent Vanhoucke, Vijay Vasudevan, Fernanda Viégas, Oriol Vinyals, Pete Warden, Martin Wattenberg, Martin Wicke, Yuan Yu, and Xiaoqiang Zheng. 2015. TensorFlow: Large-Scale Machine Learning on Heterogeneous Systems. <https://www.tensorflow.org/>. Software available from tensorflow.org.
- [2] Martin Abadi, Andy Chu, Ian Goodfellow, H. Brendan McMahan, Ilya Mironov, Kunal Talwar, and Li Zhang. 2016. Deep learning with differential privacy. In *Proceedings of the 2016 ACM SIGSAC conference on computer and communications security*. 308–318.
- [3] Mohammad Al-Rubaie and J. Morris Chang. 2019. Privacy-preserving machine learning: Threats and solutions. *IEEE Security & Privacy* 17, 2 (2019), 49–58.
- [4] Eliseo Albert, Ignacio Torres, Felipe Bueno, Dixie Huntley, Estefanía Molla, Miguel Ángel Fernández-Fuentes, Mireia Martínez, Sandrine Poujois, Lorena Forqué, Arantxa Valdivia, Carlos Solano de la Asunción, Josep Ferrer, Javier Colomina, and David Navarro. 2021. Field evaluation of a rapid antigen test (Panbio™ COVID-19 Ag Rapid Test Device) for COVID-19 diagnosis in primary healthcare centres. *Clinical Microbiology and Infection* 27, 3 (2021), 472.e7–472.e10. <https://doi.org/10.1016/j.cmi.2020.11.004>
- [5] Eugene Bagdasaryan, Omid Poursaeed, and Vitaly Shmatikov. 2019. Differential privacy has disparate impact on model accuracy. *Advances in Neural Information Processing Systems* 32 (2019), 15479–15488.
- [6] Tom Balthazar. 2018. Sharing health-data between hospitals and other care-providers: Towards legal clarity about what can be communicated to whom. *Tijdschrift voor Geneeskunde* 74 (Feb. 2018), 161–165. <https://doi.org/10.2143/TVG.74.03.2002516>
- [7] Raef Bassily, Adam Smith, and Abhradeep Thakurta. 2014. Private empirical risk minimization: Efficient algorithms and tight error bounds. In *2014 IEEE 55th Annual Symposium on Foundations of Computer Science*. IEEE, 464–473.
- [8] Mohamed Bekkar, Hassiba Khelouane Djema, and Taklit Akrouf Alitouch. 2013. Evaluation measures for models assessment over imbalanced data sets. *Journal of Information Engineering and Applications* 3, 10 (2013).
- [9] Nicholas Carlini, Chang Liu, Úlfar Erlingsson, Jernej Kos, and Dawn Song. 2019. The secret sharer: Evaluating and testing unintended memorization in neural networks. In *28th USENIX Security Symposium (USENIX Security 19)*. 267–284.
- [10] François Chollet et al. 2015. Keras. <https://keras.io>.
- [11] Muhammad EH Chowdhury, Tawsifur Rahman, Amith Khandakar, Rashid Mazhar, Muhammad Abdul Kadir, Zaid Bin Mahbub, Khandakar Reajul Islam, Muhammad Salman Khan, Atif Iqbal, Nasser Al Emadi, et al. 2020. Can AI help in screening viral and COVID-19 pneumonia? *IEEE Access* 8 (2020), 132665–132676.
- [12] Jia Deng, Wei Dong, Richard Socher, Li-Jia Li, Kai Li, and Li Fei-Fei. 2009. Imagenet: A large-scale hierarchical image database. In *2009 IEEE conference on computer vision and pattern recognition*. IEEE, 248–255.
- [13] David J Dittman, Taghi M Khoshgoftaar, Randall Wald, and Amri Napolitano. 2014. Comparison of data sampling approaches for imbalanced bioinformatics data. In *The twenty-seventh international FLAIRS conference*.
- [14] Cynthia Dwork. 2008. Differential privacy: A survey of results. In *International conference on theory and applications of models of computation*. Springer, 1–19.
- [15] Cynthia Dwork, Vitaly Feldman, Moritz Hardt, Toniann Pitassi, Omer Reingold, and Aaron Leon Roth. 2015. Preserving statistical validity in adaptive data analysis. In *Proceedings of the forty-seventh annual ACM symposium on Theory of computing*. 117–126.
- [16] Cynthia Dwork, Aaron Roth, et al. 2014. The algorithmic foundations of differential privacy. *Foundations and Trends in Theoretical Computer Science* 9, 3-4 (2014), 211–407.
- [17] Matthew Fredrikson, Eric Lantz, Somesh Jha, Simon Lin, David Page, and Thomas Ristenpart. 2014. Privacy in pharmacogenetics: An End-to-End case study of personalized warfarin dosing. In *23rd USENIX Security Symposium (USENIX Security 14)*. 17–32.
- [18] Georgi Ganev, Bristena Oprisanu, and Emiliano De Cristofaro. 2022. Robin Hood and Matthew Effects: Differential Privacy Has Disparate Impact on Synthetic Data. In *International Conference on Machine Learning*. PMLR, 6944–6959.
- [19] Kaiming He, Xiangyu Zhang, Shaoqing Ren, and Jian Sun. 2015. Spatial pyramid pooling in deep convolutional networks for visual recognition. *IEEE transactions on pattern analysis and machine intelligence* 37, 9 (2015), 1904–1916.
- [20] Kaiming He, Xiangyu Zhang, Shaoqing Ren, and Jian Sun. 2016. Deep residual learning for image recognition. In *Proceedings of the IEEE conference on computer vision and pattern recognition*. 770–778.
- [21] Trang-Thi Ho, Khoa-Dang Tran, and Yennun Huang. 2022. FedSGDCOVID: Federated SGD COVID-19 Detection under Local Differential Privacy Using Chest X-ray Images and Symptom Information. *Sensors* 22, 10 (2022), 3728. <https://doi.org/10.3390/s22103728>
- [22] Trang-Thi Ho and Yennun Huang. 2021. DPCOVID: Privacy-Preserving Federated Covid-19 Detection. *arXiv preprint arXiv:2110.13760* (2021).
- [23] Minyoung Huh, Pulkit Agrawal, and Alexei A Efros. 2016. What makes ImageNet good for transfer learning? *arXiv preprint arXiv:1608.08614* (2016).
- [24] Matthew Jagielski, Jonathan Ullman, and Alina Oprea. 2020. Auditing differentially private machine learning: How private is private SGD? *Advances in Neural Information Processing Systems* 33 (2020), 22205–22216.
- [25] Bargav Jayaraman and David Evans. 2019. Evaluating differentially private machine learning in practice. In *28th USENIX Security Symposium (USENIX Security 19)*. 1895–1912.
- [26] Daniel S. Kermany, Michael Goldbaum, Wenjia Cai, Carolina CS Valentim, Huiying Liang, Sally L. Baxter, Alex McKeown, Ge Yang, Xiaokang Wu, Fangbing Yan, et al. 2018. Identifying medical diagnoses and treatable diseases by image-based deep learning. *Cell* 172, 5 (2018), 1122–1131.
- [27] Diederik P. Kingma and Jimmy Ba. 2015. Adam: A Method for Stochastic Optimization. In *3rd International Conference on Learning Representations, ICLR 2015, San Diego, CA, USA, May 7-9, 2015, Conference Track Proceedings*, Yoshua Bengio and Yann LeCun (Eds.). <http://arxiv.org/abs/1412.6980>
- [28] Lucas Lange. 2022. Privacy-Preserving Detection of COVID-19 in X-Ray Images. In *Master's thesis*. Leipzig University.

- [29] Yann LeCun, Léon Bottou, Yoshua Bengio, and Patrick Haffner. 1998. Gradient-based learning applied to document recognition. *Proc. IEEE* 86, 11 (1998), 2278–2324.
- [30] Yugeng Liu, Rui Wen, Xinlei He, Ahmed Salem, Zhikun Zhang, Michael Backes, Emiliano De Cristofaro, Mario Fritz, and Yang Zhang. 2022. ML-Doctor: Holistic Risk Assessment of Inference Attacks Against Machine Learning Models. In *31st USENIX Security Symposium (USENIX Security 22)*. 4525–4542.
- [31] Mani Malek Esmaili, Ilya Mironov, Karthik Prasad, Igor Shilov, and Florian Tramer. 2021. Antipodes of Label Differential Privacy: PATE and ALIBI. *Advances in Neural Information Processing Systems* 34 (2021).
- [32] Brendan McMahan, Eider Moore, Daniel Ramage, Seth Hampson, and Blaise Agüera y Arcas. 2017. Communication-efficient learning of deep networks from decentralized data. In *Artificial intelligence and statistics*. PMLR, 1273–1282.
- [33] Satwik Mishra. 2017. Handling imbalanced data: SMOTE vs. random undersampling. *International Research Journal of Engineering and Technology* 4, 8 (2017), 317–320.
- [34] Zümür Müftüoğlu, M Ayyüce Kizrak, and Tülay Yildırım. 2020. Differential Privacy Practice on Diagnosis of COVID-19 Radiology Imaging Using Efficient-Net. In *2020 International Conference on INnovations in Intelligent Systems and Applications (INISTA)*. IEEE, 1–6.
- [35] Milad Nasr, Shuang Song, Abhradeep Thakurta, Nicolas Papernot, and Nicholas Carlini. 2021. Adversary instantiation: Lower bounds for differentially private machine learning. In *2021 IEEE Symposium on Security and Privacy (SP)*. IEEE, 866–882.
- [36] Ming-Yen Ng, Elaine YP Lee, Jin Yang, Fangfang Yang, Xia Li, Hongxia Wang, Macy Mei-sze Lui, Christine Shing-Yen Lo, Barry Leung, Pek-Lan Khong, et al. 2020. Imaging profile of the COVID-19 infection: radiologic findings and literature review. *Radiology: Cardiothoracic Imaging* 2, 1 (2020), e200034.
- [37] Tulin Öztürk, Muhammed Talo, Eylül Azra Yildirim, Ulas Baran Baloglu, Ozal Yildirim, and U Rajendra Acharya. 2020. Automated detection of COVID-19 cases using deep neural networks with X-ray images. *Computers in biology and medicine* 121 (2020), 103792.
- [38] Nicolas Papernot, Martín Abadi, Úlfar Erlingsson, Ian Goodfellow, and Kunal Talwar. 2016. Semi-supervised knowledge transfer for deep learning from private training data. *arXiv preprint arXiv:1610.05755* (2016).
- [39] Nicolas Papernot, Shuang Song, Ilya Mironov, Ananth Raghunathan, Kunal Talwar, and Úlfar Erlingsson. 2018. Scalable private learning with pate. *arXiv preprint arXiv:1802.08908* (2018).
- [40] Nicolas Papernot, Abhradeep Thakurta, Shuang Song, Steve Chien, and Úlfar Erlingsson. 2021. Tempered sigmoid activations for deep learning with differential privacy. In *Proceedings of the AAAI Conference on Artificial Intelligence*, Vol. 35. 9312–9321.
- [41] Md Atiqur Rahman, Tanzila Rahman, Robert Laganière, Noman Mohammed, and Yang Wang. 2018. Membership Inference Attack against Differentially Private Deep Learning Model. *Transactions on Data Privacy* 11, 1 (2018), 61–79.
- [42] Tawfikur Rahman, Amith Khandakar, Yazan Qiblawey, Anas Tahir, Serkan Kiranyaz, Saad Bin Abul Kashem, Mohammad Tariqul Islam, Somaya Al Maadeed, Susu M Zughaier, Muhammad Salman Khan, et al. 2021. Exploring the effect of image enhancement techniques on COVID-19 detection using chest X-ray images. *Computers in Biology and Medicine* (2021), 104319. <https://doi.org/10.1016/j.combiomed.2021.104319>
- [43] Sebastian Ruder. 2016. An overview of gradient descent optimization algorithms. *arXiv preprint arXiv:1609.04747* (2016).
- [44] Ahmed Salem, Yang Zhang, Mathias Humbert, Mario Fritz, and Michael Backes. 2019. ML-Leaks: Model and Data Independent Membership Inference Attacks and Defenses on Machine Learning Models. In *Network and Distributed Systems Security Symposium 2019*. Internet Society.
- [45] Reza Shokri, Marco Stronati, Congzheng Song, and Vitaly Shmatikov. 2017. Membership inference attacks against machine learning models. In *2017 IEEE Symposium on Security and Privacy (SP)*. IEEE, 3–18.
- [46] Connor Shorten and Taghi M. Khoshgoufar. 2019. A survey on image data augmentation for deep learning. *Journal of Big Data* 6, 1 (2019), 1–48.
- [47] AA Speranskaya. 2020. Radiological signs of a new coronavirus infection COVID-19. *Diagnostic radiology and radiotherapy* 11, 1 (2020), 18–25.
- [48] Mingxing Tan and Quoc Le. 2019. Efficientnet: Rethinking model scaling for convolutional neural networks. In *International conference on machine learning*. PMLR, 6105–6114.
- [49] Samuel Yeom, Irene Giacomelli, Matt Fredrikson, and Somesh Jha. 2018. Privacy risk in machine learning: Analyzing the connection to overfitting. In *2018 IEEE 31st Computer Security Foundations Symposium (CSF)*. IEEE, 268–282.
- [50] Kaichao You, Mingsheng Long, Jianmin Wang, and Michael I Jordan. 2019. How does learning rate decay help modern neural networks? *arXiv preprint arXiv:1908.01878* (2019).
- [51] Da Yu, Huishuai Zhang, Wei Chen, and Tie-Yan Liu. 2021. Do Not Let Privacy Overbill Utility: Gradient Embedding Perturbation for Private Learning. In *International Conference on Learning Representations (ICLR)*.
- [52] Longling Zhang, Bochen Shen, Ahmed Barnawi, Shan Xi, Neeraj Kumar, and Yi Wu. 2021. FedDPGAN: Federated Differentially Private Generative Adversarial Networks Framework for the Detection of COVID-19 Pneumonia. *Information Systems Frontiers* (2021), 1–13.
- [53] Min Zhu, Jing Xia, Xiaoqing Jin, Molei Yan, Guolong Cai, Jing Yan, and Gang-min Ning. 2018. Class weights random forest algorithm for processing class imbalanced medical data. *IEEE Access* 6 (2018), 4641–4652.

A PROOF OF EQUATION 2

In the following, we prove Equation (2), which is formally given in Theorem A.1. With the prerequisites of Experiment 1 and Definition 4 from [49], we adapt their Theorem 1 and corresponding proof from ϵ -DP to (ϵ, δ) -DP.

THEOREM A.1. *Let A be an (ϵ, δ) -differentially private learning algorithm, \mathcal{A} be a membership adversary, Adv^M the membership advantage of \mathcal{A} , n be a positive integer, and D be a distribution over data points (x, y) . Then we have:*

$$\text{Adv}^M(\mathcal{A}, A, n, D) \leq e^\epsilon - 1 + \delta.$$

PROOF. According to [49] Definition 4, $\text{Adv}^M(\mathcal{A}, A, n, D)$ can be expressed as the difference between \mathcal{A} 's true and false positive rates

$$\text{Adv}^M = \Pr[\mathcal{A} = 0 \mid b = 0] - \Pr[\mathcal{A} = 0 \mid b = 1], \quad (3)$$

where Adv^M is a shortcut for $\text{Adv}^M(\mathcal{A}, A, n, D)$.

Given $S = (z_1, \dots, z_n) \sim \mathcal{D}^n$ and an additional point $z' \sim \mathcal{D}$, define $S^{(i)} = (z_1, \dots, z_{i-1}, z', z_{i+1}, \dots, z_n)$. Then, $\mathcal{A}(z', A_S, n, D)$ and $\mathcal{A}(z_i, A_{S^{(i)}}, n, D)$ have identical distributions for all $i \in [n]$, so we can write:

$$\begin{aligned} \Pr[\mathcal{A} = 0 \mid b = 0] &= 1 - \mathbb{E}_{S \sim \mathcal{D}^n} \left[\frac{1}{n} \sum_{i=1}^n \mathcal{A}(z_i, A_S, n, D) \right] \\ \Pr[\mathcal{A} = 0 \mid b = 1] &= 1 - \mathbb{E}_{S \sim \mathcal{D}^n} \left[\frac{1}{n} \sum_{i=1}^n \mathcal{A}(z_i, A_{S^{(i)}}, n, D) \right] \end{aligned}$$

The above two equalities, combined with Equation 3, gives:

$$\text{Adv}^M = \mathbb{E}_{S \sim \mathcal{D}^n} \left[\frac{1}{n} \sum_{i=1}^n \mathcal{A}(z_i, A_{S^{(i)}}, n, D) - \mathcal{A}(z_i, A_S, n, D) \right] \quad (4)$$

Without loss of generality for the case where models reside in an infinite domain, assume that the models produced by A come from the set $\{A^1, \dots, A^k\}$. (ϵ, δ) -DP guarantees that for all $j \in [k]$,

$$\Pr[A_{S^{(i)}} = A^j] \leq e^\epsilon \Pr[A_S = A^j] + \delta.$$

Using this inequality, we can rewrite and bound the right-hand side of Equation 4 as

$$\begin{aligned} &\sum_{j=1}^k \mathbb{E}_{S \sim \mathcal{D}^n} \left[\frac{1}{n} \sum_{i=1}^n \Pr[A_{S^{(i)}} = A^j] - \Pr[A_S = A^j] \cdot \mathcal{A}(z_i, A^j, n, D) \right] \\ &\leq \sum_{j=1}^k \mathbb{E}_{S \sim \mathcal{D}^n} \left[(\delta + (e^\epsilon - 1) \Pr[A_S = A^j]) \cdot \frac{1}{n} \sum_{i=1}^n \mathcal{A}(z_i, A^j, n, D) \right], \end{aligned}$$

which is at most $e^\epsilon - 1 + \delta$ since $\mathcal{A}(z, A^j, n, D) \leq 1$ for any z, A^j, n , and \mathcal{D} . \square